Journal of Cluster Science (2018) 29:533–540
https://doi.org/10.1007/s10876-018-1360-z

ORIGINAL PAPER

Antiferromagnetic Coupling in a New Mn(III) Schiff Base Complex with Open-Cubane Core: Structure, Spectroscopic and Luminescence Properties

Elif Gungor[1] · Mustafa Burak Coban[2] · Hulya Kara[1,3] · Yasemin Acar[1]

Received: 8 February 2018 / Published online: 21 March 2018

Abstract
A new open-cubane Mn^{III}, $[\{(H_2O)Mn^{III}L\}\{Mn^{III}L\}]_2{\cdot}2(CH_3OH).2(CH_3CH_2OH){\cdot}2Cl$, **1** where $\mathbf{H_2L}$=[N-(2-hydroxyethyl)-3-methoxysalicylaldimine] has been synthesized and characterized by element analysis, FT-IR, solid UV–Vis spectroscopy and single crystal X-ray diffraction. The crystal structure determination shows an open-cubane tetranuclear complex. The Mn1 ($Mn1^i$) ions is hexacoordinate by NO_5 donor sets while the Mn2 ($Mn2^i$) is pentacoordinate by NO_4 donor sets. The solid state photoluminescence properties of complex **1** and its ligand $\mathbf{H_2L}$ have been investigated under UV light at 349 nm in the visible region. $\mathbf{H_2L}$ exhibits blue emission while complex **1** shows orange-red emission at room temperature. Variable-temperature magnetic susceptibility measurements on the complex **1** in the range 2–300 K indicate an antiferromagnetic interaction.

Keywords Open-cubane Mn complex · Crystal structure · Luminescence · Antiferromagnetic coupling

Introduction

The synthesis and characterization of polynuclear manganese compounds in various topologies have attracted the researcher's interest in coordination chemistry and molecular magnetism field due to remarkable properties such as catalysis, luminescence, magnetism and bioinorganic chemistry [1–4]. Manganese compounds exhibit behaviour as single-molecule magnet (SMM), below the blocking temperature, displaying magnetization hysteresis and quantum tunneling of the magnetization [5–7].They are important on the development of a catalyst for water oxidation to evolve oxygen in the bioinorganic field [8, 9]. Besides, manganese compounds can be used as fluorescent sensors for the detection of aromatic molecules. Because, the luminescence intensity is sensitive to the environment and they have absorption band in UV region, where most aromatic molecules show absorptions [10, 11].

As described in literature, manganese complexes containing Mn_4O_x cores are divided into six major classes according to the atom connectivity. These cores are adamantane, square, basket, linear, cubane, and butterfly (Scheme 1). Particularly, clusters with the Mn_4O_6 core are adamantane [11–13], square [14] and linear (2,2,2) [15–18] topologies, those with the Mn_4O_5 core are basket [19] and linear (2,1,2) [20] topologies, the Mn_4O_4 core are observed in the cubane [21–23] and linear (1,2,1) [24, 25] topologies and the Mn_4O_2 core are seen as more common in butterfly [26–28] topology. Until today, a number of Mn^{II} and mix valance Mn^{II}/Mn^{III} complexes in cubane Mn_4O_4 motifs have also been studied in great detail for their various structural and magnetic and photoluminescence properties [11, 15, 26–28]. However, to the best of our knowledge, there are no reports on the solid state photoluminescence of Mn(III) complexes.

Our research group has successfully synthesized Schiff base metal complexes with different nuclearities and

Electronic supplementary material The online version of this article (https://doi.org/10.1007/s10876-018-1360-z) contains supplementary material, which is available to authorized users.

✉ Elif Gungor
elifonly@gmail.com; egungor@balikesir.edu.tr

[1] Department of Physics, Faculty of Science and Art, Balikesir University, 10145 Balikesir, Turkey

[2] Center of Science and Technology Application and Research, Balikesir University, 10145 Balikesir, Turkey

[3] Department of Physics, Faculty of Science, Mugla Sitki Kocman University, 48170 Mugla, Turkey

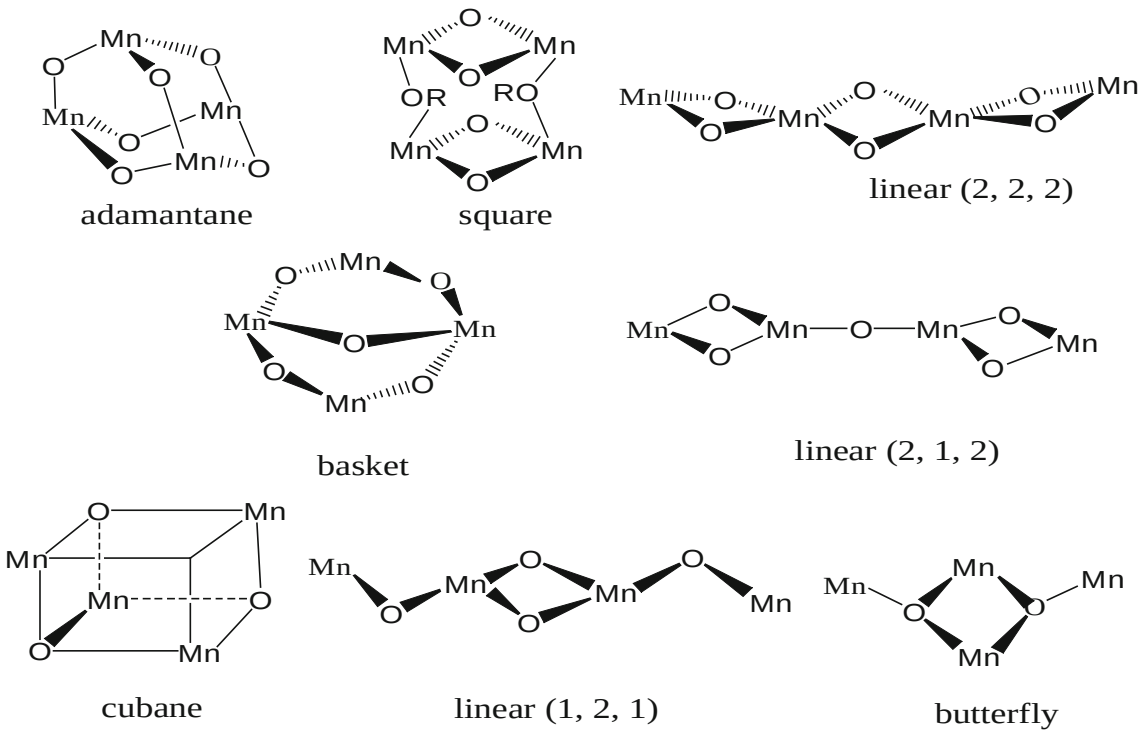

Scheme 1 Different core types observed in Mn_4O_x tetramers

investigated their magneto-structural properties [26, 27, 29–32]. Here, we report the synthesis of a new open-cubane Mn^{III} complex along with its characterization, single crystal X-ray structure, solid state UV and IR spectroscopy, solid state photoluminescence and magnetic study.

Experimental Section

Materials and Physical Measurements

All chemical reagents and solvents were purchased from Merck or Aldrich and used without further purification. Elemental (C, H, N) analyses were carried out by standard methods with a LECO, CHNS-932 analyzer. Solid-state UV–Vis spectra were measured with an Ocean Optics Maya 2000-PRO spectrometer. FT-IR spectra were measured with a Perkin–Elmer Spectrum 65 instrument in the range of 4000–600 cm^{-1}. Powder X-ray measurements were performed using Cu-K_α radiation (λ = 1.5418 Å) on a Bruker-AXS D8-Advance diffractometer equipped with a secondary monochromator. The data were collected in the range $5° < 2\theta < 50°$ in θ–θ mode with a step time of ns (5 s < n < 10 s) and step width of 0.02°. Solid state photoluminescence spectra in the visible region were measured at room temperature with an ANDOR SR500i-BL Photoluminescence Spectrometer, equipped with a triple grating and an air-cooled CCD camera as detector. The measurements were done using the excitation source (349 nm) of a Spectra-physics Nd:YLF laser with a 5 ns pulse width and 1.3 mJ of energy per pulse as the source. The temperature dependence of the magnetic susceptibility of polycrystalline samples was measured between 3 and 300 K at a field of 1.0 T using a Quantum Design model MPMS computer-controlled SQUID magnetometer. The effective magnetic moments were calculated by the equation $\mu_{eff} = 2.828\ (\chi_m T)^{1/2}$ [33] where χ_m, the molar magnetic susceptibility, was set equal to M_m/H [33]. The synthetic route of the complex is outlined in Scheme 2.

Synthesis of H_2L and Complex 1

The tridentate Schiff base ligand H_2L, was synthesized from ethanolamine (1 mmol, 0.061 ml) and 2 hydroxy-3-methoxybenzdehyde (1 mmol, 0.152 g) in a 1:1 molar ratio in hot ethanol (60 cm^3) according to the method reported previously [34]. The solution obtained was stirred at 65 °C

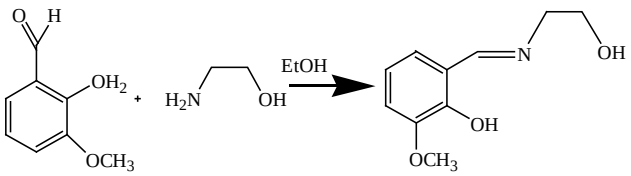

Scheme 2 The ligand $\mathbf{H_2L}$ evaluated in this study

for 10 min. The yellow compound precipitated from the solution on cooling. Analysis calculated for H_2L (yield 75%): C 54.15, H 5.05, N 7.02%. Found: C 54.11, H 5.15, N 7.10%. IR (cm^{-1}): ν(O–H) = 3175–3064, ν(C–H) = 3013–2842, υ(C=N) = 1644, υ(C–$O_{phenolic}$)- = 1241–1185. UV–Vis: λ_{max}/nm: 434.

Complex **1** was prepared by addition of manganese(II) chloride tetrahydrate (1 mmol, 0.197 g) in 20 cm^3 of hot methanol to the ligand (1 mmol, 0.195 g) in 30 cm^3 of hot ethanol. To the resulting solution was then added triethylamine (Et_3N) (1 mmol, 0.101 ml). This solution was warmed to 78 °C and stirred for 15 min. The resulting solution was filtered rapidly and then allowed to stand at room temperature. Several weeks of standing was led to the growth of brown crystals of the title compound suitable for X-ray analysis. Analysis calculated for $C_{46}H_{68}Cl_2Mn_4N_4O_{18}$ (yield 70%): C 43.99, H 5.46, N 4.46%. Found: C 43.90, H 5.48, N 4.33%. IR (cm^{-1}): *ν*(O–H) = 3175–3064, *ν*(C–H) = 3013–2842, υ(C=N) = 1614, υ(C–$O_{phenolic}$)- = 1477–1409, υ(H_2O) = 865–814. UV–Vis: λ_{max}/nm: 488.

X-ray Structure Determination

Diffraction measurements were made on a Bruker Apex II kappa CCD diffractometer using graphite monochromated Mo-K_α radiation (λ = 0.71073 Å) at 100 K for **1**. In the Olex2 program [35], the structure was solved by direct methods using SHELXS [36] and refined by full-matrix least-squares based on $|F_{obs}|^2$ using SHELXL [37]. The non-hydrogen atoms were refined anisotropically, while the hydrogen atoms, generated using idealized geometry, were made to "ride" on their parent atoms and used in the structure factor calculations. The crystallographic data for 1 are summarized in Table 1. The selected bond lengths and angles are listed in Table 2. Crystallographic data for the structural analyses have been deposited with the Cambridge Crystallographic Data Centre, CCDC No. 1818226. These data can be obtained free of charge via www.ccdc.cam.ac.uk.

Results and Discussion

Crystal Structure

The asymmetric unit of the tetranuclear manganese complex **1** includes one $[\{(H_2O)Mn^{III}L\}\{Mn^{III}L\}]^{+2}$ molecule, one ethanol and one methanol molecules and two Cl^{2-} ion. The crystal structure determination shows that complex **1** is an open-cubane structure with two missing vertices consisting of two dinuclear $[Mn_2^{III}L_2(H_2O)]$ subunits as shown in Fig. 1. The coordination environments and geometry of the manganese ions are different. The Mn1 ($Mn1^i$) ion (i = − *x*+2, *y*, −*z*+1/2) is hexacoordinate by NO_5 donor sets in which one imine nitrogen atom, two alkoxy and two phenoxy oxygen atoms and one oxygen atom of the methoxy group from the Schiff base ligands. Mn1 ($Mn1^i$) atom has a distorted octahedral geometry. The basal average Mn–O bond distances are in the range 1.936 (4)–1.993 (4) Å, while the axial bond distances are 2.476 (4) Å owing to the Jahn–Teller distortions at the d^4 metal center. The Mn2 ($Mn2^i$) is pentacoordinate by NO_4 donor sets in which two alkoxy and one phenoxy oxygen atoms of the Schiff base ligands and one oxygen atom of the water molecule. The Addison distortion index of Mn2 ($Mn2^i$) atom was found as $\tau = 0.0011$, which indicates that Mn2 ($Mn2^i$) atom is close to a square pyramidal geometry [31, 38]. The basal average Mn–N bond distances and Mn–O–Mn bridging bond angles for **1** are 1.940(6)–1.944(6) Å and 72.78(16)–90.57(18)°. The intramolecular Mn···Mn distances vary from 3.165 to 3.881 Å. The selected bond lengths and bond angles for the complex **1** are given in Table 2 which is comparable to those of the similar complex reported in the literature [8].

The crystal packing of tetranuclear Mn(III) complex shows that the neighboring tetramer are linked through intramolecular and intermolecular O–H···O, C–H···O, C–H···Cl, O–H···Cl and O–H···O hydrogen bonds (Table 3). These tetramers are arranged in one-dimensional polymeric chain structure along the [001]. Hydrogen-bonded polymeric network lies in the *ab* plane (Fig. 2). Additionally, 1D polymeric structure with hydrogen bond interactions may enhance the stability of the solid-state structure of **1** and generate 3-D networks (Fig. S1).

Oxidation states of Mn1 ($Mn1^i$) and Mn2 ($Mn2^i$) ions have been assigned on the basis of bond valence sum analysis [39, 40] and consideration of bond lengths. Bond-valence-sum calculations (Table 2) suggest that both Mn1 ($Mn1^i$) and Mn2 ($Mn2^i$) are in a 3 + oxidation state [40].

X-ray Powder Diffraction Pattern

Before proceeding to the spectroscopic, photoluminescence and magnetic characterization, we note that experimental powder X-ray patterns for **1** are well in position with those of simulated patterns on the basis of single crystal structure of **1** (Fig. S2).

FTIR Spectra

The IR spectra of $\mathbf{H_2L}$ and **1** provide information about the metal-ligand bonding. The IR spectra of **1** shows in comparison with that of its free ligand $\mathbf{H_2L}$ in Fig. S3. The strong sharp absorption at 1644 cm^{-1} in spectra of $\mathbf{H_2L}$ can be assigned to C=N stretch [31, 41]. This band in **1** is

Table 1 Details of the data collection and refinement parameters for complex

Empirical formula	$C_{46}H_{68}Cl_2Mn_4N_4O_{18}$
Formula weight	1255.70
Crystal system	Monoclinic
Space group	*C*2/*c*
a/Å	24.0840(5)
b/Å	19.6299(4)
c/Å	11.8110(2)
α/°	90
β/°	19.6299(4)
γ/°	90
Volume/Å^3	4895.13(17)
Z	4
ρ_{calc} g/cm^3	1.704
μ/mm^{-1}	1.199
Θ range for data collection/°	2.8–27.6
Index ranges	$-31 \le h \le 31, -25 \le k \le 21, -15 \le l \le 15$
Reflections collected	33027
Independent reflections	5594
Data/restraints/parameters	5594/44/326
Goodness-of-fit on F^2	1.04
Final R indexes [I >=2σ (I)]	R_1 = 0.090, wR_2 = 0.255

Table 2 Selected bond lengths (Å), angles (°) for **1** and bond valance sum (BVS) calculations for the Mn ions

Mn1–N1	1.940 (6)	Mn2–N2	1.944 (6)
Mn1–O1	1.968 (4)	Mn2–O1	1.936 (4)
Mn1–O1^i	2.476 (4)	Mn2–O4	2.010 (5)
Mn1–O2	1.904 (5)	Mn2–O5	2.304 (5)
Mn1–O6^i	1.993 (4)	Mn2–O6	1.962 (4)
Mn1–O7^i	2.439 (5)		
O1–Mn1–O1^i	84.19 (15)	O7^i–Mn1–O1^i	144.22 (16)
O1–Mn1–O6^i	90.57 (18)	O1–Mn2–O4	98.40 (2)
O1–Mn1–O7^i	91.37 (17)	O1–Mn2–O5	95.90 (2)
O2–Mn1–O1^i	92.64 (17)	O1–Mn2–O6	86.84 (17)
O2–Mn1–O1	175.70 (2)	O4–Mn2–O5	92.20 (3)
O2–Mn1–O6^i	91.30 (2)	O6–Mn2–O4	174.60 (2)
O2–Mn1–O7^i	92.90 (2)	O6–Mn2–O5	88.67 (19)
O6^i–Mn1–O1^i	72.78 (16)		
O6^i–Mn1–O7^i	71.79 (17)		

	Oxidation state of Mn 3+
Mn1 (Mn1^i)	2.88
Mn2 (Mn2^i)	2.73

Symmetry code: (i) $-x+2, y, -z+1/2$

shifted to at 1614 cm^{-1} frequency attributed to the coordination of the imine nitrogen. The **H_2L** ligand is show a band at 3175–3064 cm^{-1} for their stretching vibrations of aromatic *ν*(O–H) which disappears in **1** indicating deprotonation of the Schiff base upon complexation. Several absorption bands occurred in the range 3013–2842 cm^{-1} are ascribed to the aromatic and aliphatic *ν*(C–H) stretches. The C–$O_{phenolic}$ group of **H_2L** indicates a strong band in the range 1241–1185 cm^{-1} while this band in **1** is observed in the range 1477–1409 cm^{-1} which indicate that deprotonated phenolic oxygen atoms coordinate to the metal centre [42]. The IR spectra of υ(H_2O) of coordinated water appeared at 865–814 cm^{-1}, indicating the binding of water molecules to the metal ions [43]. These findings are in good agreement with our previously published transition metal complexes [31, 44, 45].

Solid State UV–Vis Spectra

A solid-state electronic absorption spectrum of **H_2L** and **1** was recorded (Fig. S4). The electronic spectra of **H_2L** showed absorption bands at 488 nm while complex **1** displayed in 434 nm. The absorption band of the complex **1** is shifted to lower wavelength region compared with their parent ligand. The reason for this shift is the coordination of oxygen and nitrogen atoms of the ligand with manganese(III) ions. This band at the high energy region is probably obscured by the intense charge transfer transitions. The absorption band could be assigned to π → π* or n → π* transition of the ligand [46].

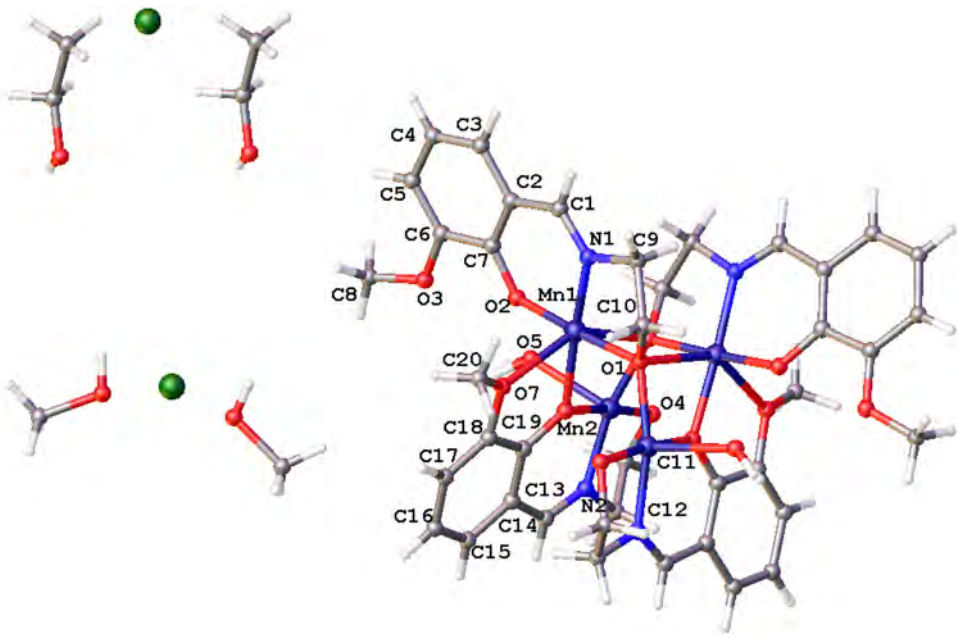

Fig. 1 Molecular structure of **1**. Symmetry code: (i) $-x+2, y, -z+1/2$

Table 3 Hydrogen bond and short-contact geometry (Å,°) for **1**

D–H···A*	D–H	H···A	D···A	D–H···A	Symmetry
O5–H5A···O9	0.90	1.87	2.658	145	1 + x, 1 − y, 1/2 + z
O5–H5B···O8	0.90	2.23	2.945	137	1 − x, y, 3/2 − z
O5–H5B···Cl2	0.90	2.50	3.305	148	1 + x, y, z
O9–H9···O3	0.84	2.54	3.117	127	1 − x, 1 − y, − z
O9–H9···O5	0.84	2.16	2.658	118	1 + x, 1 − y, − 1/2 + z
C1–H1···O8	0.95	2.58	3.342	137	1 + x, 1 − y, − 1/2 + z
C8–H8B···O9	0.98	2.42	3.140	130	1 − x, 1 − y, − z
C21–H21A···O9	0.98	1.83	2.800	174	− x, 1 − y, 1 − z
C21–H21B···O4	0.98	1.52	2.460	157	− 1 + x, y, z
C22–H22B···Cl1	0.98	2.23	3.060	141	–

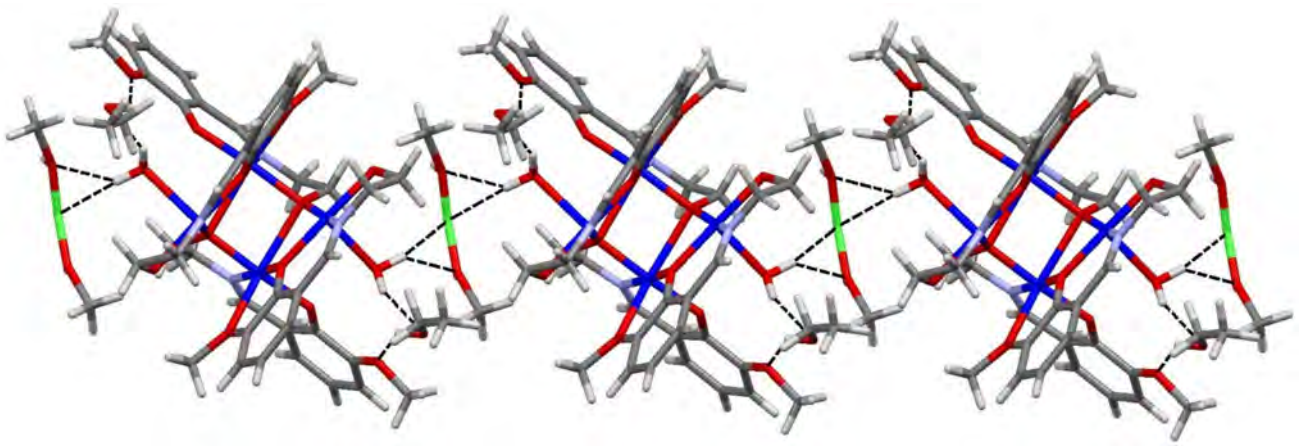

Fig. 2 Intramolecular and intermolecular hydrogen bonds connect the molecules which form a one-dimensional polymeric chain structure in complex **1**

Luminescent Properties

Coordination compounds have been reported to have ability to adjust the emission wavelength of organic materials through incorporation of metal centers which impetus us to investigate the photoluminescence properties [47, 48]. Because of enhanced stability of metal complexes compared to organic counterparts, coordination polymers are used as photoluminescent materials [10, 49]. Therefore, it is important to investigate the luminescence properties of coordination compounds in view of potential applications as light-emitting diodes (LEDs).

The solid-state photoluminescence properties of **H_2-L** and **1** have been investigated at room temperature in the visible regions upon excitation at λ_{ex} = 349 nm (Fig. 3). It is obvious that **H_2L** displays a strong blue emission band at λ_{max} = 437 nm which is attributable to the n → π or π → π* electronic transition (ILCT) [50, 51]. The stronger emission band in **1** is at λ_{max} = 661 nm. This band may be ascribed to a charge-transfer transition between ligands and metal centers, namely ligand-to-metal charge transfer (LMCT) [41, 44]. The observed emission spectrum of **1** is red shifted when compared with that of **H_2L** which is caused by its microenvironment and electronic energy transfer [2]. So, the complex 1 emits strong orange-red light. The chelation of the ligand **H_2L** to Mn(III) also increases the rigidity of the **H_2L** and thus reduces the vibration of **1** molecules, so that the excited energy of complex **1** molecules cannot be easily released by thermal energy [52].

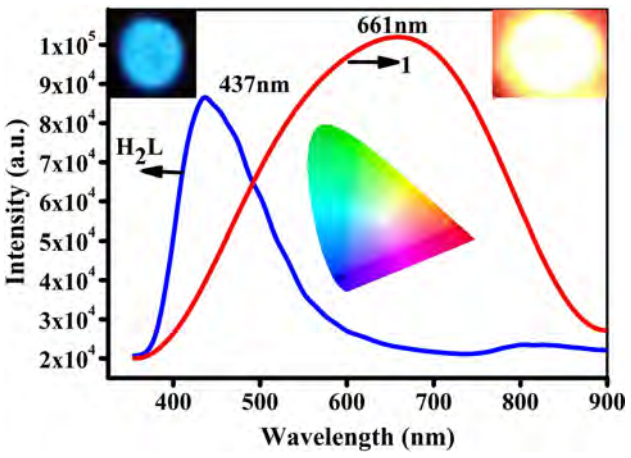

Fig. 3 The emission spectrum of **H_2L** ligand and **1** in solid samples at room temperature ($\lambda_{exc.}$ = 349 nm). (Inset figures Upper-left photo is photoluminescent image of H_2L, upper-right photo is photoluminescent image of 1, while excited at 349 nm and middle photo is CIE chromaticity diagram image of H_2L and **1**.)

Magnetic Properties

Variable-temperature magnetic susceptibility data were collected on a powdered microcrystalline sample of **1** (Fig. 4) in the temperature range 2–300 K under an applied field of 0.1 T. The molar magnetic susceptibility of the tetranuclear Mn(III) unit increases with decreasing temperature. The χ_mT values of 10.96 cm^3 K mol^{-1} at 300 K is slightly lower than the spin-only values of 12.00 cm^3 K mol^{-1} for four uncoupled Mn(III) ions based on g = 2.0. When the temperature is lowered, the curve shows a continuous decay tending to a plateau at temperatures below 10 K. The value at 1.9 K is 3.57 cm^3 K mol^{-1}. This behavior is indicative of a weak antiferromagnetic coupling. The drop in the $\chi_m T$ product below 8 K suggests the presence of magnetic anisotropy expected for Mn(III) ions, inter- or more likely intramolecular antiferromagnetic couplings [3].

In order to qualitatively evaluate the magnitude of the magnetic interaction between the Mn(III) ions, the magnetic model of **1** was simplified by employing the same intramolecular magnetic coupling constant (*J*) for the comparatively complicated case (Fig. 5). In addition, the intermolecular magnetic interaction (zJ') was taken into account. The experimental magnetic susceptibility data for **1** were analyzed by using the following isotropic Hamiltonian Eq. (1).

$$H = -J(S_1S_2 + S_2S_3 + S_3S_4 + S_1S_4) \quad (1)$$

The temperature dependence of the magnetic susceptibility is given by the Eq. (2):

$$\chi_t = \frac{Ng^2\beta^2}{2kT}\frac{A}{B} \quad (2)$$

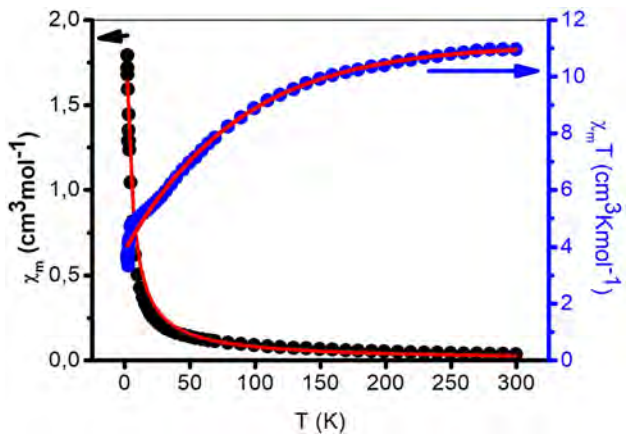

Fig. 4 Temperature dependence of χ_M versus T and $\chi_M T$ versus T for **1**. The solid line represents the best fit of the experimental data based on the Heisenberg model

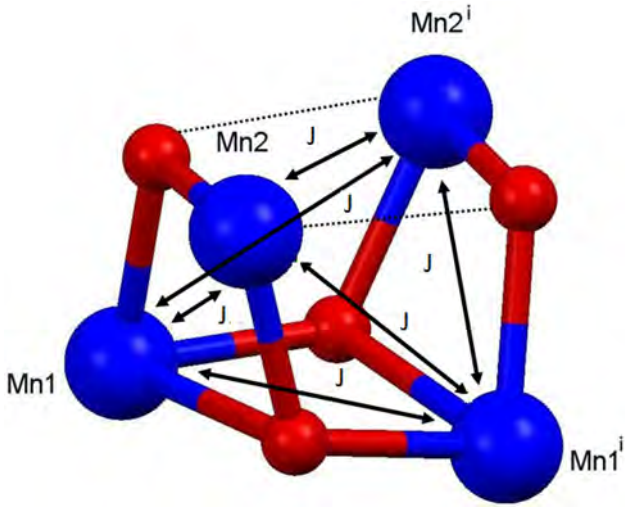

Fig. 5 A view of the Mn_4O_4 core of **1** with the exchange coupling pattern

$$
\begin{aligned}
A &= 408exp(48J/kT) + 840exp(32J/kT) \\
&\quad + 1092exp(18J/kT) + 1100exp(6J/kT) \\
&\quad + 900exp(-4J/kT) + 476exp(-12J/kT) \\
&\quad + 160exp(-18J/kT) + 24exp(-22J/kT) \\
B &= 17exp(48J/kT) + 45exp(32J/kT) \\
&\quad + 78exp(18J/kT) + 110exp(6J/kT) \\
&\quad + 135exp(-4J/kT) + 119exp(-12J/kT) \\
&\quad + 80exp(-18J/kT) + 36exp(-22J/kT) \\
&\quad + 5exp(-24J/kT)
\end{aligned}
$$

$$\chi_m = \frac{\chi_t}{1 - \chi_t\left(\frac{2zJ'}{Ng^2\beta^2}\right)} \tag{3}$$

where N, g, μ_B, k, T have their usual meanings, χ_t is molar susceptibility per $Mn(III)_4$ unit only including intramolecular magnetic coupling. The best–fit parameters obtained by least squares fit through Eq. (3) are as follows: $J = -0.197 \pm 0.0012\ cm^{-1}$, $zJ' = -0.022 \pm 0.0015\ cm^{-1}$, $g = 2.1 \pm 0.0064$, with $R = 0.9848$ (R is the agreement factor defined as $R = \sum(\chi_{obsd} - \chi_{cald})^2 \Big/ \sum(\chi_{obsd})^2$). These results indicate the presence of weak antiferromagnetic exchange interaction between Mn(III) ions for **1**.

Conclusions

In this work, we presented crystal structure, photoluminescence and magnetic characterization of a new open-cubane Mn^{III} complex. The dc magnetic properties of **1** was found to be in good agreement with the literature, and analysis of the data using χ_mT and isotropic spin Hamiltonian model dictates a weak antiferromagnetic coupling in the complex. The solid-state photoluminescence measurements display remarkable orange-red emission for **1** and blue emission for its ligand, $\mathbf{H_2L}$, which is attributable to the $n \rightarrow \pi$ or $\pi \rightarrow \pi^*$ electronic transition (ILCT). In addition, the complex **1** characterized in this study is a first example of Mn(III) Schiff base complex which show luminescence properties. Furthermore, the complex exhibits a strong orange-red luminescence emission in the solid state at room temperature as seen from the (CIE) chromaticity diagram, and hence the complex may be a promising orange-red OLED developing electroluminescent material for flat panel display applications.

Acknowledgements The authors are grateful to the Research Funds of Balikesir University (BAP–2017/200) for the financial support and Balikesir University, Science and Technology Application and Research Center (BUBTAM) for the use of the Photoluminescence Spectrometer. The authors are also very grateful to Prof. Dr. Andrea Caneschi (Laboratory of Molecular Magnetism, Department of Chemistry, University of Florence) for the use of SQUID magnetometer and helpful suggestions.

References

1. T. G. Carrell, S. Cohen, and G. C. Dismukes (2002). *J. Mol. Catal. A Chem.* **187**, 3.
2. J. Liu, Z. Liu, S. Yuan, and J. Liu (2013). *J. Mol. Struct.* **1037**, 191.
3. N. Hoshino, T. Ito, M. Nihei, and H. Oshio (2003). *Inorg. Chem. Commun.* **6**, 377.
4. L. P. Nitha, R. Aswathy, N. E. Mathews, B. Sindhu Kumari, and K. Mohanan (2014). *Spectrochim. Acta Part A Mol. Biomol. Spectrosc.* **118**, 154.
5. W. Wernsdorfer, N. Aliaga-Alcalde, D. N. Hendrickson, and G. Christou (2002). *Nature* **416**, 406.
6. D. Gatteschi and R. Sessoli (2003). *Angew. Chem. Int. Ed.* **42**, 268.
7. S. Mandal, G. Rosair, J. Ribas, and D. Bandyopadhyay (2009). *Inorg. Chim. Acta* **362**, 2200.
8. C. Lee and C. M. Aikens (2015). *J. Phys. Chem. A* **119**, 9325.
9. H. Hou (2011). *Materials (Basel)* **4**, 1693.
10. S. Q. Zang, L. H. Cao, R. Liang, H. W. Hou, and T. C. W. Mak (2012). *Cryst. Growth Des.* **12**, 1830.
11. J. K. Nath, A. Mondal, A. K. Powell, and J. B. Baruah (2014). *Cryst. Growth Des.* **14**, 4735.
12. R. Zhang, Z.-H. Ni, L.-F. Zhang, and H.-Z. Kou (2014). *Bull. Korean Chem. Soc.* **35**, 1965.
13. C. E. Dubé, D. W. Wright, S. Pal, P. J. Bonitatebus, and W. H. Armstrong (1998). *J. Am. Chem. Soc.* **120**, 3704.
14. M. K. Chan and W. H. Armstrong (1991). *J. Am. Chem. Soc.* **113**, 5055.
15. J. Yoo, A. Yamaguchi, M. Nakano, J. Krzystek, W. E. Streib, L. Brunel, H. Ishimoto, G. Christou, and D. N. Hendrickson (2001). *Inorg. Chem.* **40**, 4604.
16. D. Li, H. Wang, S. Wang, Y. Pan, C. Li, J. Dou, and Y. Song (2010). *Inorg. Chem.* **49**, 3688.
17. P. J. Bettle, L. N. Dawe, M. U. Anwar, and L. K. Thompson (2011). *Eur. J. Inorg. Chem.* 5036.
18. E. A. Karlsson, B.-L. Lee, T. Åkermark, E. V. Johnston, M. D. Kärkäs, J. Sun, Ö. Hansson, J.-E. Bäckvall, and B. Åkermark (2011). *Angew. Chem. Int. Ed.* **50**, 11715.

19. S. Mukhopadhyay, J. Staples, W. H. Armstrong, and R. Purdue (2002). *Chem. Commun.* **4**, 864.
20. H. Chen, J. W. Faller, R. H. Crabtree, and G. W. Brudvig (2004). *J. Am. Chem. Soc.* **126**, 7345.
21. C. Mn, V. Mckee, and W. Shepard (1985). *J. Chem. Soc. Chem. Commun.* **4**, 158.
22. J. Z. Wu, E. Sellitto, G. P. A. Yap, J. Sheats, and G. C. Dismukes (2004). *Inorg. Chem.* **43**, 5795.
23. G. Aromí, S. Bhaduri, P. Artús, K. Folting, and G. Christou (2002). *Inorg. Chem.* **41**, 805.
24. Z. S. Bai, Z. P. Qi, Y. Lu, Q. Yuan, and W. Y. Sun (2008). *Cryst. Growth Des.* **8**, 1924.
25. H. Chen, M.-N. Collomb, C. Duboc, G. Blondin, E. Rivière, J. W. Faller, R. H. Crabtree, and G. W. Brudvig (2005). *Inorg. Chem.* **44**, 9567.
26. C. C. Stoumpos, N. Lalioti, I. A. Gass, K. Gkotsis, A. A. Kitos, H. Sartzi, C. J. Milios, C. P. Raptopoulou, A. Terzis, E. K. Brechin, and S. P. Perlepes (2009). *Polyhedron* **28**, 2017.
27. L. B. Jerzykiewicz, J. Utko, M. Duczmal, P. Starynowicz, and P. Sobota (2010). *Eur. J. Inorg. Chem.* **28**, 4492.
28. C. C. Beedle, C. J. Stephenson, J. Katie, W. Wernsdorfer, D. N. Hendrickson, and K. J. Heroux (2008). *Inorg. Chem.* **47**, 10798.
29. H. Kara (2007). *Z. Naturforsch.* **62**, 691.
30. Y. Yahsi and H. Kara (2014). *Spectrochim. Acta Part A Mol. Biomol Spectrosc.* **127**, 25.
31. Y. Yahsi, E. Gungor, M. B. Coban, and H. Kara (2016). *Mol. Cryst. Liq. Cryst.* **637**, 67.
32. H. K. Ara and H. Kara (2008). *Anal. Sci.* **24**, 79.
33. O. Kahn *Molecular Magnetism* (VCH Publishers, New York, 1993).
34. E. Gungor and H. Kara (2015). *J. Struct. Chem.* **56**, 1646.
35. O. V. Dolomanov, L. J. Bourhis, R. J. Gildea, J. A. K. Howard, and H. Puschmann (2009). *J. Appl. Crystallogr.* **42**, 339.
36. G. M. Sheldrick (2008). *Acta Crystallogr. A* **64**, 112.
37. G. M. Sheldrick (2015). *Acta Crystallogr. Sect. C Struct. Chem.* **71**, 3.
38. A. W. Addison, T. N. Rao, J. Reedijk, J. van Rijn, and G. C. Verschoor (1984). *J. Chem. Soc. Dalton Trans.* 1349.
39. G. J. Palenik (1997). *Inorg. Chem.* **36**, 4888.
40. W. Liu and H. H. Thorp (1993). *Inorg. Chem.* **32**, 4102.
41. C. Kocak, G. Oylumluoglu, A. Donmez, M. B. Coban, U. Erkarslan, M. Aygun, and H. Kara (2017). *Acta Crystallogr. Sect. C Struct. Chem.* **73**, 414.
42. Z.-L. You and H.-L. Zhu (2004). *Z. Für Anorg. Und Allg Chem.* **630**, 2754.
43. E. S. Aazam, A. F. EL Husseiny, and H. M. Al-Amri (2012). *Arab. J. Chem.* **5**, 45.
44. E. Gungor (2017). *Acta Crystallogr. Sect. C Struct. Chem.* **73**, 393.
45. E. Gungor, S. Celen, D. Azaz, and H. Kara (2012). *Spectrochim. Acta Part A Mol. Biomol. Spectrosc.* **94**, 216.
46. A. B. Lever *Inorganic Electronic Spectroscopy, Vol. 33, Studies in Physical and Theoretical Chemistry* (Elsevier, Amsterdam, 1984).
47. X.-Z. Guo, Z.-Y. Zhang, Z.-L. Li, S.-S. Shi, and S.-S. Chen (2017). *Crystals* **7**, 73.
48. S.-S. Chen, Q. Liu, Y. Zhao, R. Qiao, L.-Q. Sheng, Z.-D. Liu, S. Yang, and C.-F. Song (2014). *Cryst. Growth Des.* **14**, 3727.
49. K. H. He, W. C. Song, Y. W. Li, Y. Q. Chen, and X. H. Bu (2012). *Cryst. Growth Des.* **12**, 1064.
50. A. Donmez, M. B. Coban, C. Kocak, G. Oylumluoglu, U. Baisch, and H. Kara (2017). *Mol. Cryst. Liq. Cryst.* **652**, 213.
51. A. Donmez, G. Oylumluoglu, M. B. Coban, C. Kocak, M. Aygun, and H. Kara (2017). *J. Mol. Struct.* **1149**, 569.
52. B. Valeur *Molecular Fluorescence: Principles and Application* (Wiley-VCH, Weinheim, 2002).